UNIVERSITY OF LIVERPOOL

UNIVERSITY OF LIVERPOOL

SCHOOL OF ENGINEERING

AERO420 - AEROSPACE CAPSTONE GROUP DESIGN PROJECT

FLIGHT TEST READNIESS REVIEW

Elevated Attitude

MEng/MSc Aerospace Engineering

May 2021

Name	Position
George Jones	Project Lead
Oliver Brown	Avionics Lead
Benjamin Buxton	Avionics Team
Amanda Reeve	Avionics Team
Oliver Miller	Airframe Design Lead
John McEvoy	Airframe Design CAD Technician
Ryan Davidson	Airframe Design Team
Stuart Roberts	Airframe Design Team
Harry Thomas	Payload Lead
Hriday Agrawal	Payload Team
Alexander Parr	Payload Team
Daniel Flanagan	Simulation Team

School of Engineering, University of Liverpool Brownlow Hill, Liverpool, L69 3GH

Executive Summary

The purpose of this FTTR is to set out the various systems and structural tests that have been performed in order to ensure the UAV is ready for its maiden flight.

Tests have been carried out on the airframe structure; wing and tail tests at high load factor have proven that the carbon spars used in the design can withstand the maximum load factor of 1.15 in the chosen flight envelope. Various systems test of the avionics components, such as the PX4 flight controller, have been performed along with ensuring the custom airframe build operates as expected.

System control tests were carried out in preparation of the flight tests, informing the pilot of handling characteristics. A risk analysis was conducted in the form of a risk register – this identified and ranked the risks in terms of their severity and likelihood and allowed the team to highlight the biggest threats to project success. Both mitigation and contingency plans were put in place to prevent and deal with any risks that could have potentially occurred.

A comprehensive set of Flight Reference Cards have been provided with the aircraft to allow for proficient, safe testing to be carried out by the customer. These include everything from unboxing the aircraft to emergency procedures.

RAF Woodvale has been chosen as a provisional location for the first flight test, given the large area of the grounds as well as the facilities that are specifically designed to accommodate aircraft.

The total spend of the project is £638.03 of the £1000 budget.

Table of Contents

Table of Abbreviations

Abbreviation	Description
AR	Aspect Ratio
CAD	Computer Aided Design
CG	Centre of Gravity
FEA	Finite Element Analysis
FMU	Functional Mock-up Unit
GB	Giga Byte
GPS	Global Positioning System
GSD	Ground Sample Distance
GSD	Ground Sampling Distance
MB	Mega Byte
MTOW	Maximum Take-Off Weight
NDT	Non-Destructive Testing
QGC	QGroundControl
SD	Secure Digital
STOL	Short Take-off and Landing
STOL	Short Take Off and Landing
UAV	Unmanned Air Vehicle
USB	Universal Serial Bus

Applicable Documents

Document Reference	Description
AVI_PL_AVI_001	Iron bird images
AVI_TEST_AVI_001	Interactive avionics test
AVI_TEST_CALCS_001	Control surface deflection calculations
AVI_TEST_FM_001	Flight mode test selection
AVI_TEST_WIND_001	Wing tunnel testing – control surface test rig and full wing
DES_FI_CALCS_001	Tail plane forces and manoeuvre limits
DES_PL_ALL_001	FRC's
DES_TEST_BUILD_001	Build document
DES_TEST_BUILD_002	Manufacturing documentation
DES_TEST_MNGT_001	Design change log
MNGT_FI_RISK_001	Risk register of entire project
MNGT_FI_RISK_002	Risk of flight test
PAY_CAMERA_TEST_001	Sony A5000 camera testing
PAY_CAMERA_TEST_002	Sony A5000 camera trigger test
PAY_CAMERA_TEST_003	Sony A5000 camera manual settings test
PAY_GIMBAL_TEST_001	Gimbal test
PKG_TEST_RISK_001	Packaging standards
SIM_FI_CALCS_001	Simulink model calculations & MATLAB
SIM_TEST_WIND_001	Wind tunnel scale model

1 Introduction

1.1 Problem Statement

The main aim set by the customer was:

To study the Great Cormorant (Phalacrocorax carbo carbo) bird species, located on Puffin Island.

This was to be achieved by addressing three main objectives:

1. Count the quantity of Cormorant nests on Puffin Island in the summer breeding season.
2. Identify the location of all Cormorant nests on Puffin Island.
3. Assess the change in number of Puffin Island Cormorant nests during the summer.

Based on the team's experience, a fixed wing UAV was selected to serve as a transport medium for a camera payload system. This platform would allow the team to meet the three objectives stipulated above.

2 System Definition

2.1 Design Overview

The UAV, Elevated Attitude, presented in the final design review, has completed its manufacture stage to the specifications outlined, with changes to the platform confined to optimising the overall design. The fixed-wing UAV, with particulars shown in Table 1 and Figure 1 went through an iterative design process starting with conceptualisation to meet the highest-level requirements; preliminary, to give the aircraft dimensional correctness and a final design which focused on the interfacing between sub-systems. This process involved all stakeholders to ensure that modules, once manufactured, would meet the requirements set out by the project. The success of this design process is self-evident in supporting document DES_TEST_BUILD_001, which, pictorially shows the module manufacture and their subsequent successful integration with each other.

Table 1 - Physical characteristics of UAV

Parameter	Value	Unit
Wingspan	2.4	[m]
Overall Length	1.54	[m]
Standing Height	0.61	[m]
AR	8	n.d
Propeller Diameter	0.279	[m]
Max Take Off Weight (MTOW)	6.5	[kg]

Table 2 - Performance characteristics of UAV

Parameter	Value	Unit
Range	72	[km]
Endurance	85	[min]
Stall Speed (Un-flapped)	10.2	[m/s]
Stall Speed (Flapped)	8.6	[m/s]
Take-off Speed (Flapped)	10.3	[m/s]
Take-off Speed (Un-Flapped)	12.2	[m/s]
Manoeuvre Speed	14	[m/s]
Survey Mission Speed	13	[m/s]

The aircraft's performance characteristics can be seen in Table 2, calculations are provided for reference in applicable document DES_FI_CALCS_001. A key parameter of note is that of the reduced stall speed whilst utilising the onboard flaps. A reduction of 1.6 m/s could be significant in missions where STOL (Short Take Off and Landing) distances are required. The position of the CG (Centre of Gravity), relative to the centre-of-pressure and landing gear, is important for stability both on the ground and in the air. The tail dragger configuration needs the CG located behind the wheels contact point with the ground, and to provide a stable platform, must be located in front of the main-wing quarter chord. To achieve the desired location, the CG can be fine-tuned by adjusting the longitudinal position of the gimbal, the CG location can be seen below in Figure 1.

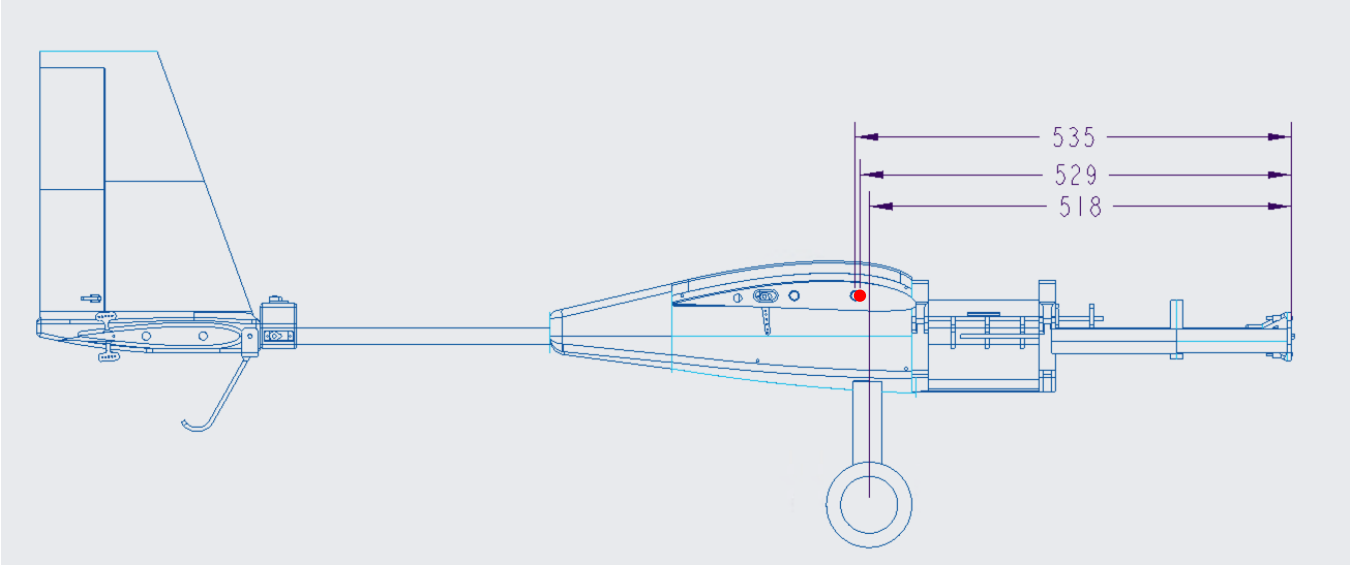

Figure 1 - Side view of aircraft with CG position labelled with respect to the nose of the UAV

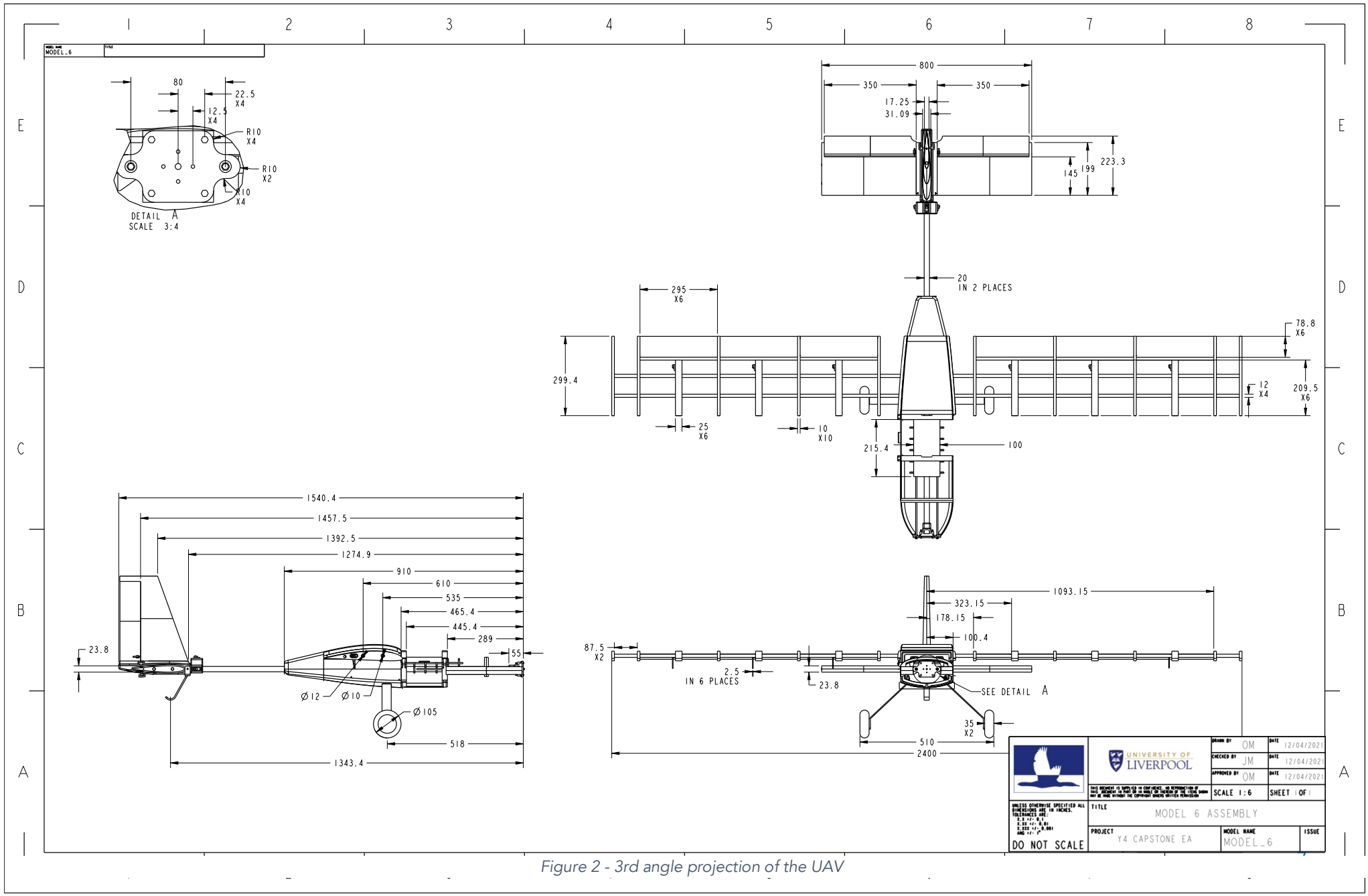

Figure 2 - 3rd angle projection of the UAV

2.2 Avionics Overview

The selection of the avionics components is detailed below in Figure 2, it displays an overview of the avionics architecture and the interfacing of the components with the Pixhawk 4 computer. The architecture displayed requires a custom airframe configuration which is discussed in detail below. All the subsystems have undergone rigorous testing procedures and analysis, see section 5.4.

2.2.1 Avionics Architecture

The Pixhawk 4 flight controller acts a central hub for the majority of the avionics components to connect to. Figure 3 shows the avionics architecture and how each of the selected components connect.

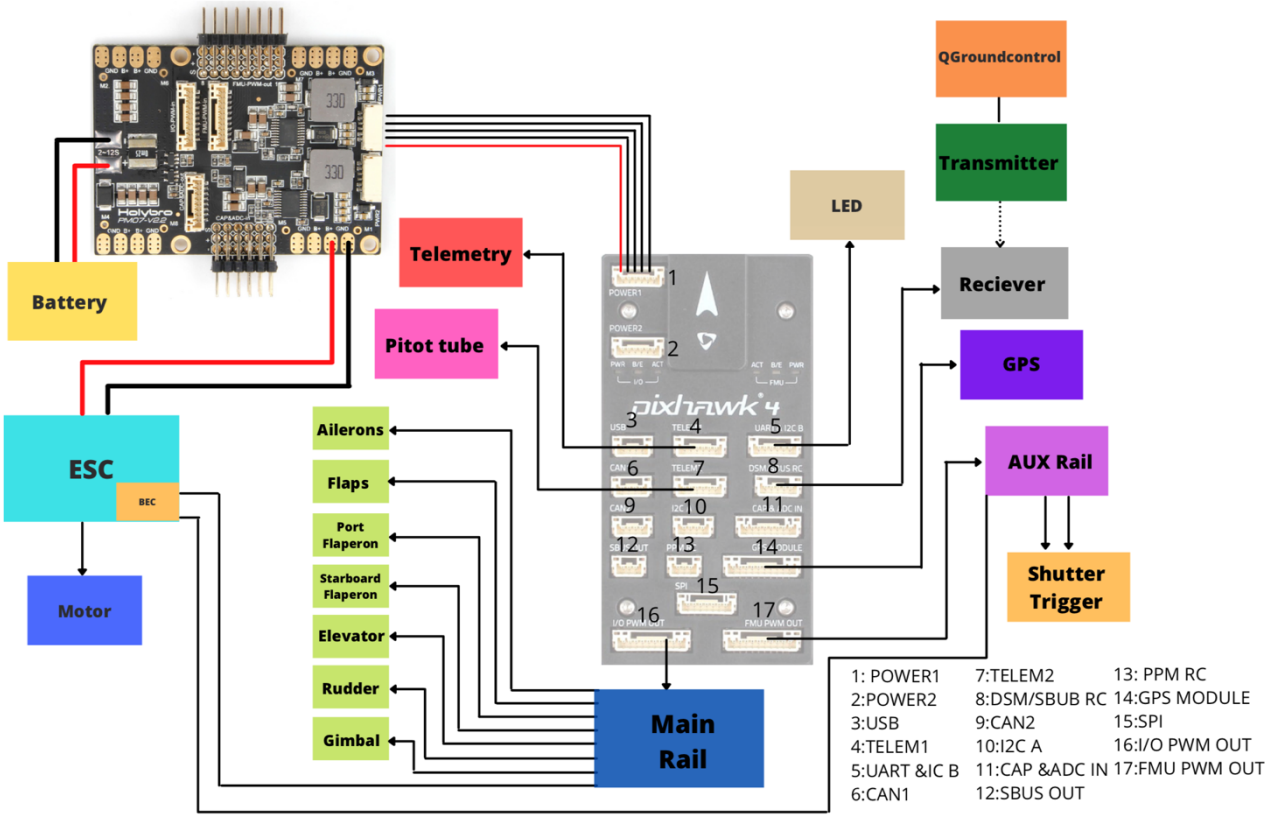

Figure 3 - Avionics components wire drawing

2.2.2 Custom Airframe Configuration

As the UAV does not conform to any of the PX4 firmware standard vehicle layouts, a custom airframe setup was built to match the design of the aircraft. This included all flight surfaces, a one axis gimbal and a camera shutter. The building of the custom software consisted of two files: a mixer file and a configuration file. The entire process of the custom build is shown in document AVI_FI_PX4_001.

The wings consisted of three control surfaces: inboard flaps, mid wing flaperons and conventional ailerons. The custom airframe has been designed such that the flaperons mimic the position of the two-stage flaps and are adjusted by 25% of the input received from the ailerons. 25% was selected as

a conservative starting point and will be iterated through the flight tests, as detailed in Section 4.5, to achieve a desirable amount of roll control authority.

2.2.3 Propulsion System

The team concluded the 4-max PO-3547-1190, as shown in Figure 4 in the middle, with a mass of 154g, and constant power of 1190kv would provide sufficient thrust for the UAV. The high power to weight ratio is favourable since the aircraft will be operating from a grass airfield. The high-performance motor will shorten the take-off distance. Paired with the PO-3547-1190 motor, the APCE 11" x 5.5° propellor in Figure 4, on the right, was selected. The propellor is 11 inches in diameter, with 5.5° of twist.

Figure 4 - Selected motor (left) propeller (right)

2.3 Payload Overview

2.3.1 Camera System

The camera system consists of a Sony A5000 camera with a f/1.8 aperture prime lens to produce 0.52 cm/pixel GSD images at 60 meters from the imaging target. This system is linked to the Pixhawk 4 via the Seagull Hot Shoe connector utilising aux pins 5 and 6 on the FMU pin board with the other end connecting to the camera via its USB-C port. The camera will be triggered via QGroundControl, specifically from waypoints on a custom flight plan for the survey, with the image capture rate being approximately once every 1.5 seconds to get the overlap necessary. The images will be stored on an SD card capable of write rates of 90 MB/s and a size of 128GB. The key settings for the camera will be an ISO of 100 and exposure of between 1/80 and 1/2000. A dummy camera fitting the dimensions of the actual camera and lens was created for the initial flight test run to make sure the payload would not be damaged; an image can be seen in Section 6.2.2 Figure 30. Figure 5 shows the final camera and lens selection.

Figure 5- Sony A5000 (left) and 50mm f1.8 lens (right)

2.3.2 Gimbal System

The final gimbal system provides one axis of rotation and is capable of 90° of rotation from vertical in both directions utilising a single servo motor which easily allows the 46° that is required for this mission. The gimbal system is affixed directly to the forward carbon spar and is located under the avionics tray. It received several design iterations to improve its rotational capabilities and make sure there is room for the cables that trigger the camera. CAD models of the final design can be seen in Figure 6.

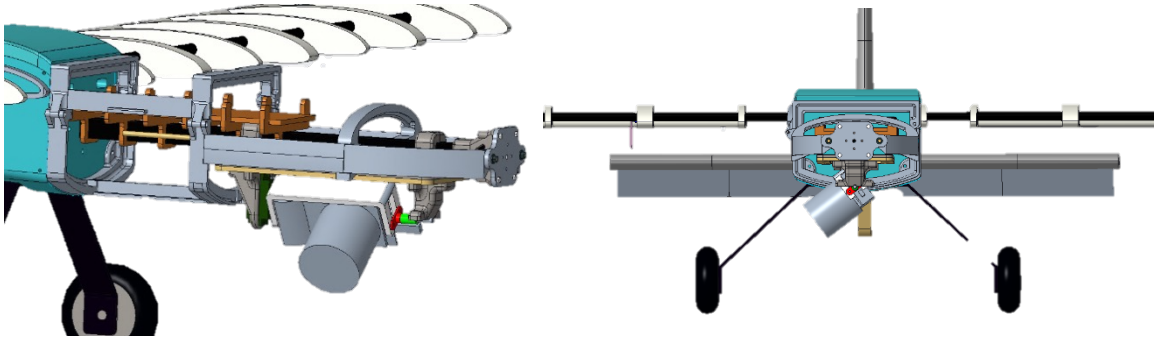

Figure 6 - Side and front view of assembled gimbal on airframe model.

3 Changes Since FDR

3.1 Change Control Process

A change control process was implemented by the project team to ensure that all change requests were recorded, and sense checked before being adopted into the design. Figure 7 shows the change

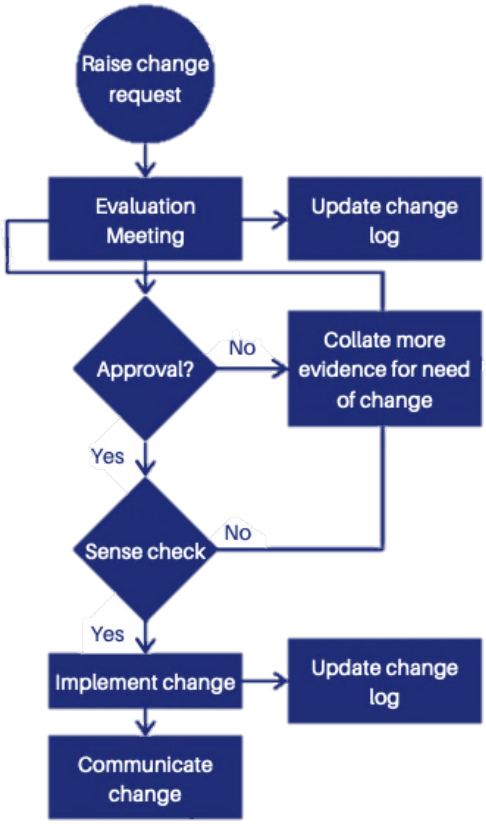

Figure 7 - Change control process implemented by the project team

control process used throughout the project. This process was inspired by the Association for Project Management control process but has been changed to suit the scale of this project. The change log can be seen in document DES_TEST_MNGT_001. Following this process ensures that all decisions made are in the best interests of the project and are backed by evidence and logic. Involving multiple stakeholders in the decision also ensures that any interfacing issues can be identified before the implementation.

3.2 Design Amendments

From the change control process outlined in section 3.1, 10 changes have been made since the FDR. These changes are shown in Table 3.

Table 3 - Changes made since the FDR

UID	Change	Description	Date of Approval
CS01	Servo orientation	Servos to be changed from rotating in the horizontal plane to rotating in the vertical plane.	10/03/2021
CS02	Control horn duality	Two control horns to be used instead of the originally proposed one. This is to ensure that the control surface can sustain the loads in both deflection direction.	17/03/2021
CS03	Elevator carbon spar diameter increase	Elevator carbon spar to be increased in diameter to match that of the rudder. Changing from 2mm to 5mm	01/04/2021
CS04	Outboard aileron servo repositions (one wing)	One large rib to be mirrored around its longitudinal axis such that the servo will protrude on the opposite side.	5/04/2021
CS05	Torsion Bar Diameter reduction	Torsion bars used on the forward spar to be reduced in diameter such that M3 cap head screws can be used.	15/04/2021
CS06	Tail Modularity	The Tail module has been sub-sectioned into 2 parts to further aid transportability.	20/04/2021
CS07	Tail Servo Sleeve	Tail servo housing to be changed to incorporate a dual servo set-up for the elevators	20/04/2021

CS08	Tail Support Sleeve	Tail Support sleeve to be changed to a slide-on design to aid the insertion of the M5 X40 fixing bolt.	20/04/2021
CS09	Forward Cowling manufacturing method	Forward cowling to be changed from a solids structure to a shell wrapped in Groupner foam to aid in weight reduction	04/05/2021
CS10	Wing Lights	Port (Red) and Starboard (Green), lights were added to the wing tips to aid visual flight orientation	06/05/2021

4 Simulated Testing

Before the UAV can be declared ready for flight it was necessary to perform some finite element analysis on key parts of the aircraft. This was performed on Creo Simulate. The purpose of this is to ensure the structure will not fail in flight/testing. The key areas studied were the main wings and the tail section. The models were loaded from CREO parametric directly into the CREO Simulate software package. As both of this software are part of the same PTC package, the transition between the two was seamless and allowed for an exact representation of the wing to be used.

The main wings were analysed to ensure the structure could withstand the upwards lift force that would be generated. The primary failure mode we were concerned with was shearing of the carbon spars at the root of the wing.

When analysing the tail structure there were a number of failure methods we needed to consider. Firstly, could the forces have produced by the horizontal and vertical tail cause shearing of the rods at the root? Secondly, could the forces generated by the rudder cause twisting of the main rear square cross section leading to crack propagation and shearing.

The design specification requires a platform which possesses flight handling characteristics such that a qualified remote pilot can operate it with ease. In aircraft design it is imperative to understand the flight handling characteristics before undertaking any operational flight tests so that they can be predicted and controlled. As a result, flight tests can be performed safely, and resources can be saved on expensive operational flight tests that could result in project setbacks.

4.1 Wing FEA

An FEA analysis was carried out by the team on the wing structure. Initially the wing was isolated from the rest of the UAV to ensure the simulation ran correctly. Once this was done the whole aircraft was simulated with a total lift force of 65N across the wings. This is based on the calculations outlined in applicable document DES_FI _CALCS_001. The simulation setup is shown in Figure 8.

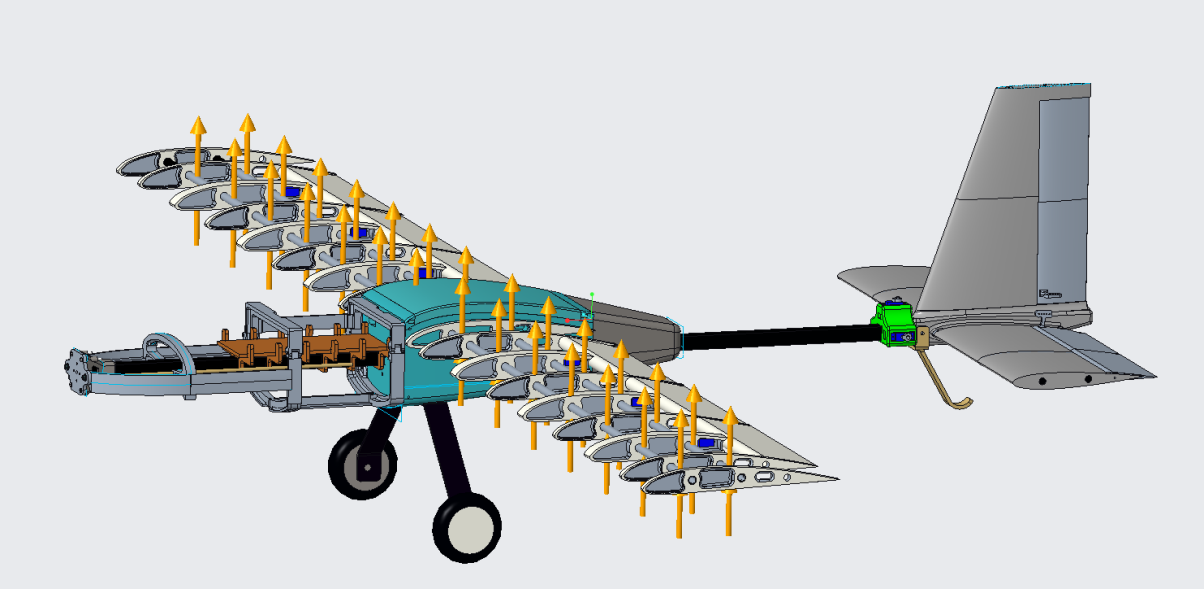

Figure 8 - Simulation set up from Creo Simulate

Shown in Figures 9 and 10 is the results of the FEA analysis of the wing. It was determined that the wing would deflect a maximum of 30mm, and the maximum shear stress experienced by the wing is 44.6MPa.

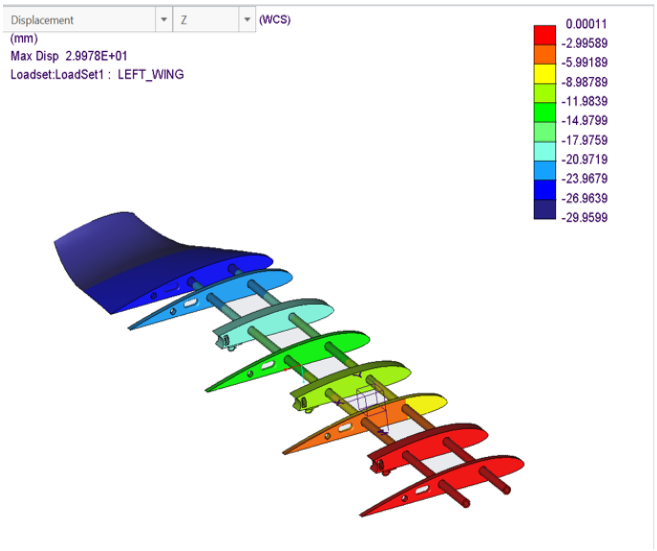

Figure 9: FEA analysis of the wing structure at normal load conditions using CREO Simulate

The ultimate tensile strength of the woven carbon fibre rods is quoted as 65MPa by the manufacturer (Easy Composites, 2021). This gives a factor of safety of 1.45.

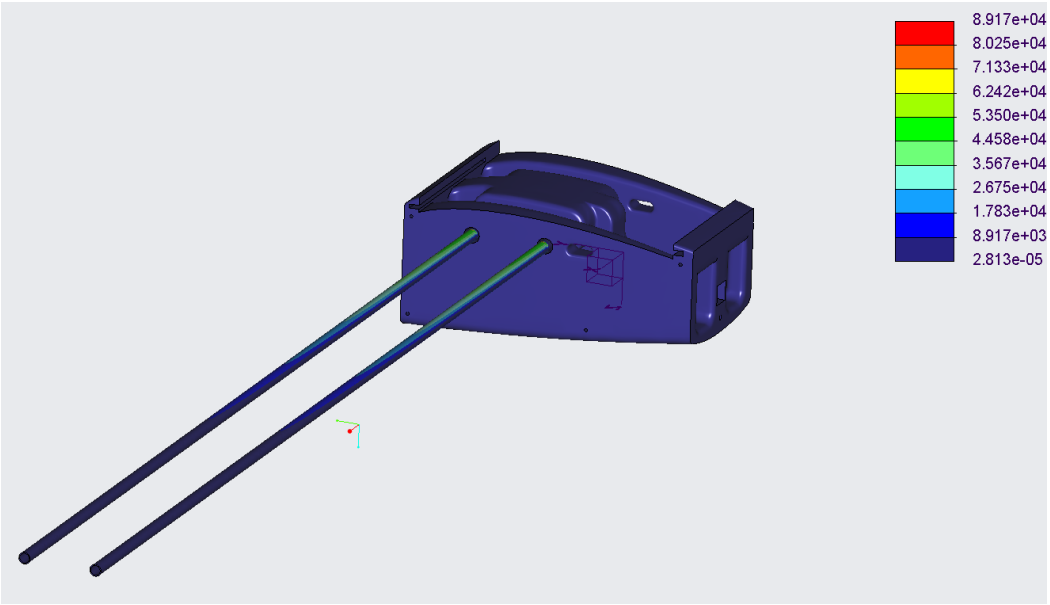

Figure 10: Section Cut of UAV showing maximum shear stress

4.2 Tail FEA

Similarly, the tail section was imported into CREO Simulate and an FEA analysis was conducted by the team. To assume worst case scenario maximum rudder and elevator was simulated. The simulation setup is shown below in Figure 11.

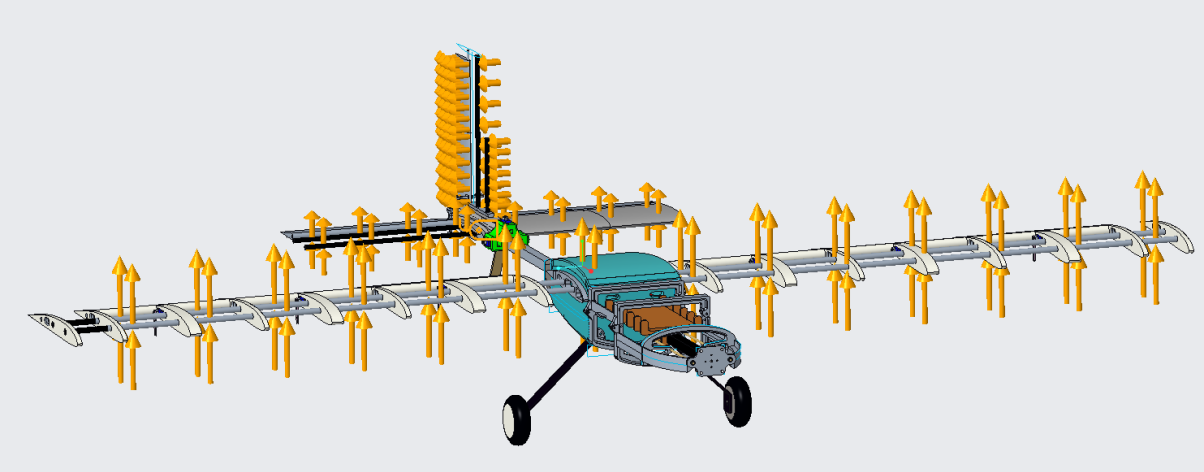

Figure 11 - Simulation set up for Creo simulate (tail)

The results of this analysis are shown in Figure 12.

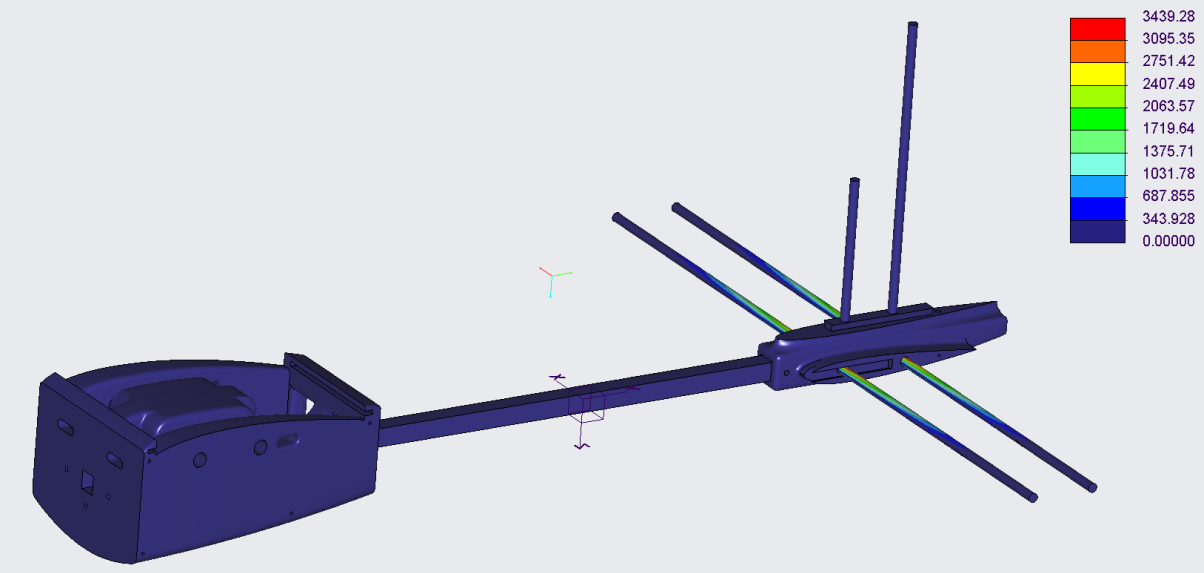

Figure 12 - FEA results for tail section of UAV showing shear force along the horizontal spars

The horizontal tail was found to have a maximum shear stress of 3.4MPa and a tip deflection of 2.3mm. This is consistent with our initial estimates since the total lift force produced by the tail with maximum elevator deflection was 7.84N, see applicable document DES_FI_CALCS_001. The primary failure mode of the horizontal would come from shearing of the rod due to deflection of the beam. The carbon fibre rods are quoted to 65MPa giving a safety factor in excess of 19.

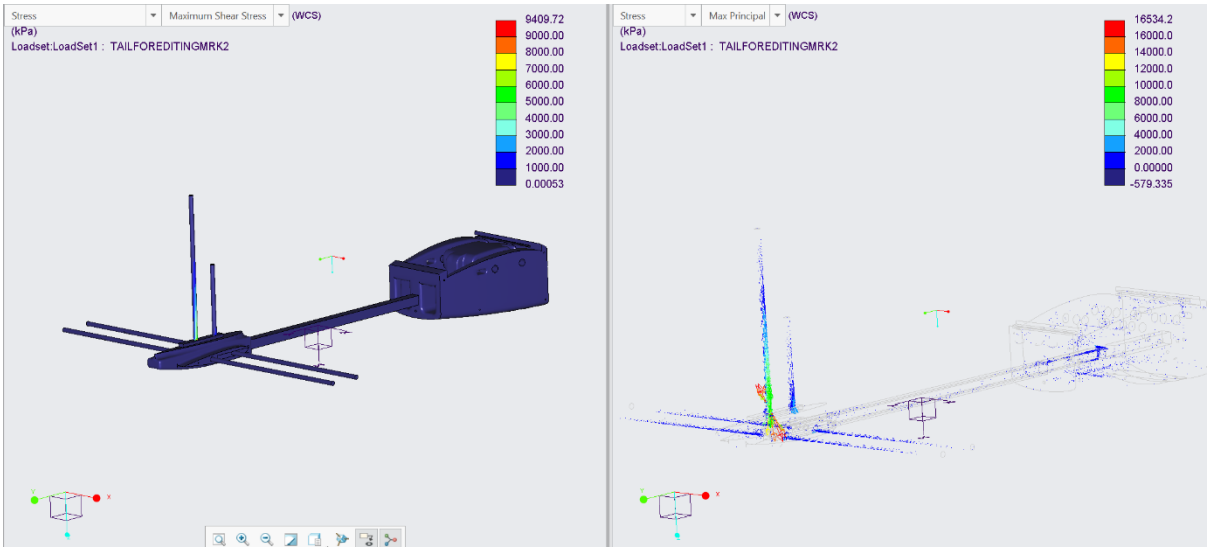

Figure 13 - FEA results showing maximum shear and principal stress

Figure 13 shows the vertical spars are subjected to greater stress. The maximum principal stress occurs at the root of the spars where they connect with the tail module. At this point the maximum principal stress is 16.5MPa with a maximum shear stress of 9.4MPa. This gives a safety factor of 3.9. As can be seen from Figure 13, little stress is translated from the horizontal and vertical spars to the main tail spar. Furthermore, there was no twist observed in the tail spar in CREO Simulate.

In order to validate these FEA wing and tail results, a number of physical tests were conducted. These can be seen in Section 5.

4.3 Avionics Testing

All of the avionics components were examined in terms of their power draw provided by the supplier. This was then used to determine a maximum theoretical power draw of 89.1W predominantly from the motor. The two batteries arranged in parallel, provide the circuit with 11.1V at a capacity of 12,000mAh. This leads to a total operational time of 90 minutes before the batteries are no longer capable of providing sufficient power to the avionics. Document AVI_PL_CALCS_001 contains the calculations related to the aforementioned results.

4.4 Flight Control Testing (MATLAB/Simulink)

The six degree of freedom MATLAB/Simulink state space model presented in Appendix A is used for the non-linear modelling and linearization of the platforms control system based on an input-output feedback loop. The control design was verified using real time simulation by analysing the states of the aircraft as a result of the dynamic pilot inputs. The inputs are captured via a joystick controller which are visualized using the Simulink built-in animation tool from the Aerospace blockset. To ensure a robust flight control design the model requires the platforms aerodynamic characteristics for the different flight conditions, motor thrust values, the inertial tensor matrix and physical sizing parameters. The data was obtained using wind tunnel testing, verified using historical data and physical testing, see document SIM_FI_CALCS_001.

The objectives of the model include the verification of:

- Aircraft stability at cruise speed (To ensure sufficient resolution images OCDR1)
- Suitable flight handling qualities so a qualified pilot can operate it with ease (FCDR3)
- Max control inputs for safe flight conditions to inform the pilot notes/brief
- Trim conditions for straight and level flight at cruise

Some assumptions/limitations of the model include that the platform has a rigid body, propulsion is non-zero and instantaneous and that the propeller is not aerodynamic and provides thrust along the centre line. The control surface deflection is also instantaneous and the flaperon inputs are discounted, air density remains constant and that the coefficient of lift of the wing and body is only a function of angle of attack and neglects reverse stall conditions.

Inputting throttle to 50% with no stick inputs resulted in the aircraft stabilizing at a cruise velocity of approximately 13ms^{-1}, the velocity at which the platform will be capturing images during the survey. The plots shown in Figure 14 show longitudinal pitch oscillations as the aircraft settles at the desired speed, with the maximum pitch angle just exceeding 6.2°. The aircraft state is predictable and can readily controlled by the pilot. The stabilization to a steady state means that the platform will be able to meet the stability requirement for capturing images during the survey and that the aircraft can be handled with ease and demonstrate the stability of the aircraft. Convergent behaviour is observed; hence it may be assumed that the aircraft performs at least in Straight and Level conditions.

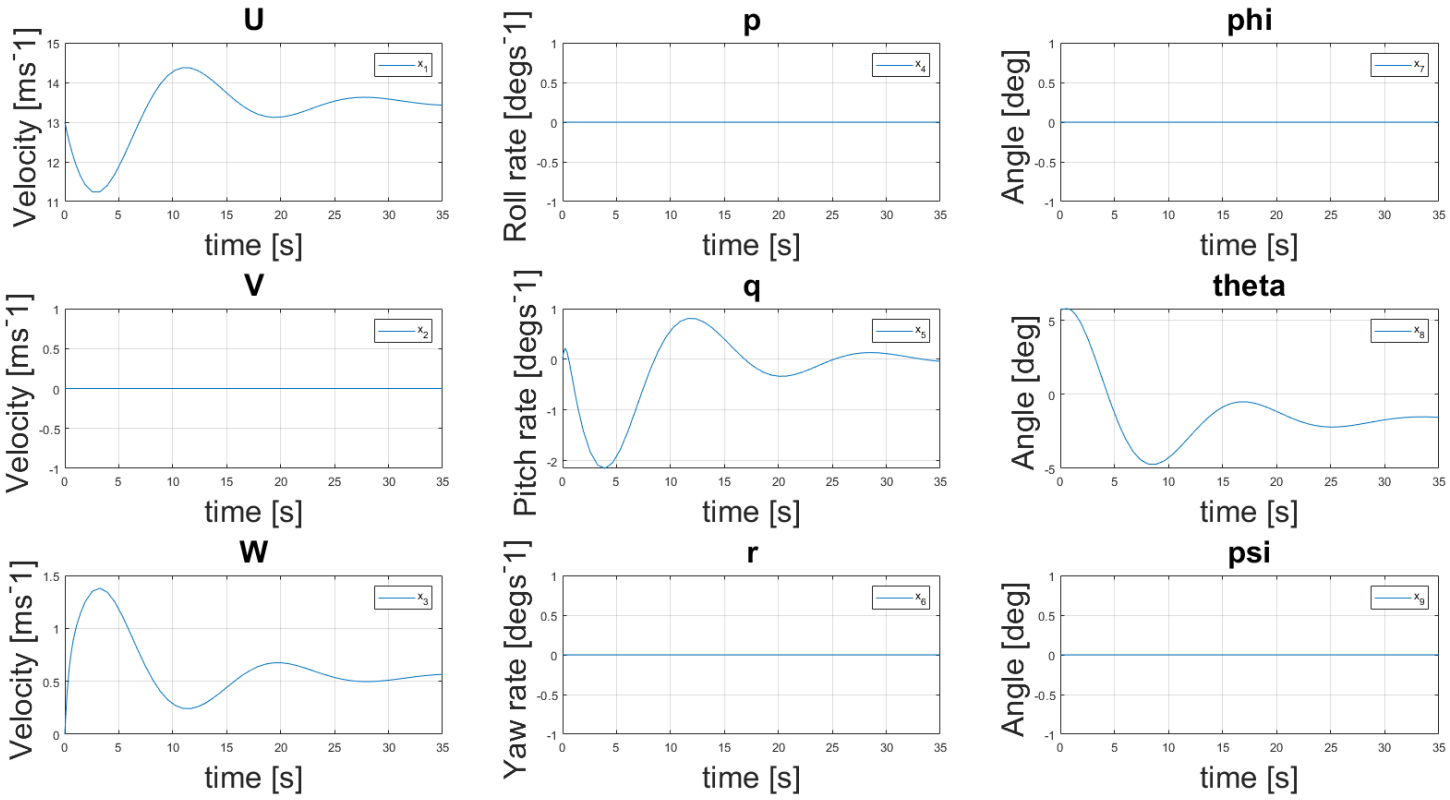

Figure 14 - The nine state outputs of the Simulink model at cruise

The platform at no point must exceed a bank angle of 20°, it has been calculated in document DES_FI_CALCS_001 to show that there will be insufficient lift produced at this angle and would result in loss of control or a crash. Using the model, we can predict the control inputs that would result in exceeding the maximum bank angle and use this to prevent such from occurring. Figure 15 shows that a 3.5s full stick aileron deflection of °30 from straight and level flight results in the platform banking to 20°, the pilot should take this into consideration when unfamiliar with the handling characteristics, this will be documented in the pilot notes in the flight brief.

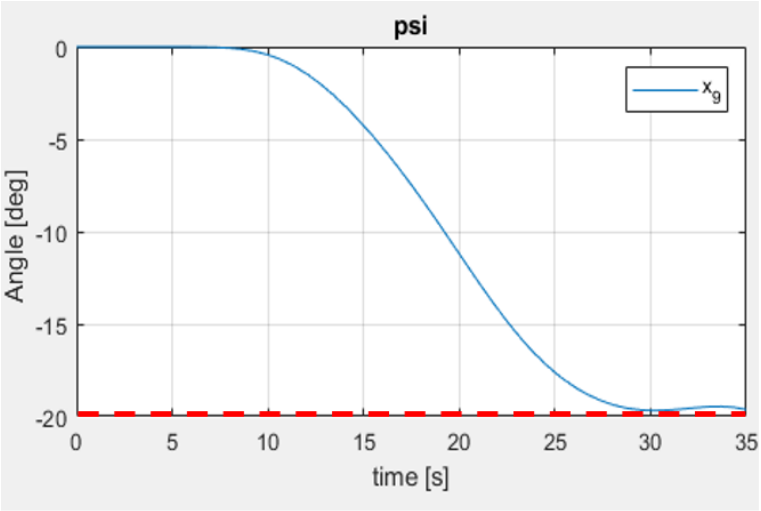

Figure 15 - Max aileron step input to maximum allowable bank angle (red)

Figure 16 shows that a 2s full stick elevator deflection of 30° from straight and level flight results in the platform pitching to 15°, this will also be documented in the pilot brief. This angle has been determined to be the max allowable pitch before stall while allowing a factor of safety of 1.5.

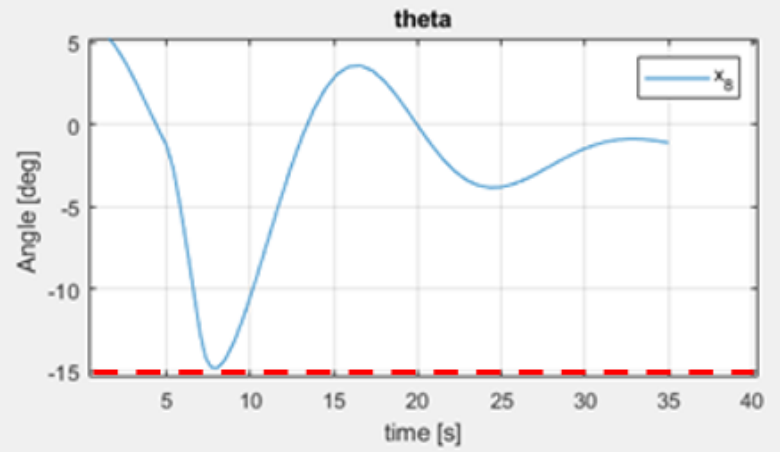

Figure 16 - Max Elevator step input to maximum allowable pitch angle (red)

The Simulink model can also determine the trim conditions by optimising the aircraft states and control inputs at the equilibrium point. It uses the MATLAB Fminsearch function to find the minimum control inputs required for steady state, straight and level flight. The aircraft was trimmed at cruise conditions and the following control inputs shown in Table 4 were determined to be optimal. This can be input into the Taranis flight controller for optimised cruise conditions and for an extended range flight the code for this can be found in SIM_FI_CALCS_001.

Table 4 - Trim values at cruise conditions, values ≤ 1e-4 are considered negligible

Model output	Parameters	Values at trim condition
X1	U velocity [m/s]	12.99
X2	V velocity [m/s]	-5.05e-08
X3	W velocity [m/s]	0.85
X4	p Roll rate [rad/s]	-7.1e-07
X5	q Pitch rate [rad/s]	-2.8e-08
X6	r yaw rate [rad/s]	-2.8e-08
X7	**Φ** roll Euler angle [rad]	-2.8e-08
X8	**Θ** pitch Euler angle [rad]	0.0149
X9	**Ψ** Yaw Euler angle [rad]	-6.03e-08
U1	Aileron input required [rad]	-6.3e-08
U2	Horizontal stabilizer input required [rad]	-0.32
U3	Rudder input required [rad]	0.012
U4	Throttle input required [rad]	0.012

The overall recommendation to the flight testers was that the aircraft would fly based upon simulated results. The pilot should take note of the handling characteristics demonstrated in the simulation before the test flights are completed to mitigate risks as mentioned in MNGT_FI_RISK_002.

5 Physical Testing

5.1 Wing Structural Testing

To test if the wings of the aircraft are able to deflect the amount predicted by the FEA without failure, a physical wing test was conducted. The aim of the test was to assess the strength of the carbon spars used in the wing structure; these spars bear the bending and shear loads induced in the wings. Due to limited resources, a full wing model could not be constructed for the test (including skin, ribs, control surfaces etc), therefore a model consisting of just the two main wing spars was used. However, this model is an accurate representation of the real wing structure as the wings have been designed such that most of the wing loading is borne by the two main carbon spars. Figure 17 shows the free body diagram of the experimental set-up.

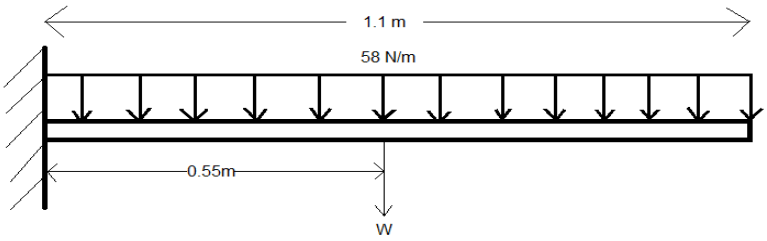

Figure 17 - Free body diagram of wing loading

The weight of the spars, W = 1.53 N, is negligible in comparison to the wing loading (W = 2.4% of total loading).

Figure 18 is the experimental set up and method used to test the wing deflection.

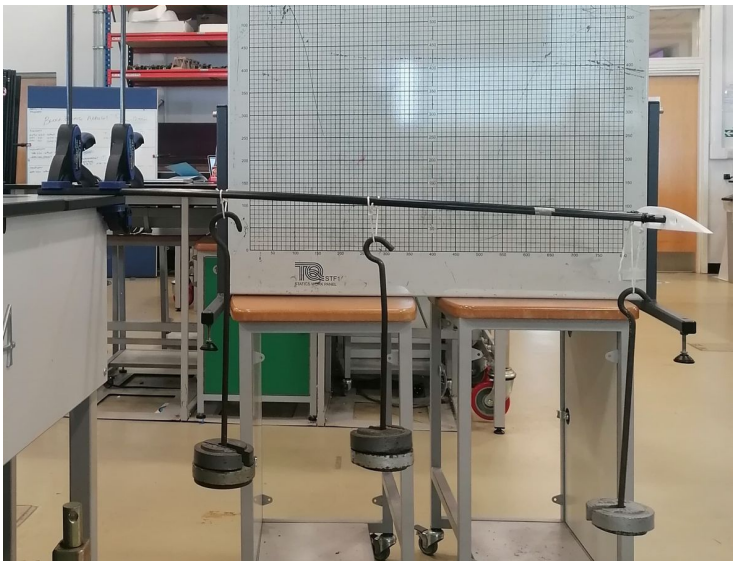

Figure 18 - Experimental set-up and qualitative results of the physical wing testing

- A 12mm diameter carbon fibre rod was cut into two spars of length 1.2m each (to replicate the wing structure).
- A single rib was used at the tip of the spars to maintain a realistic separation distance between the spars.
- The spars were clamped to the test bench to replicate the root of the wing as it connects to the wing box, with 1.1m of the spars forming the cantilever shown in Figure 18.
- Three wires were attached to the spars along the span of the model from which weights could be hung.
- Two 2 kg weights and one 1.5kg weight were hung from left to right along the wingspan to mimic a distributed lifting load.
- This 5.5kg weight distribution is indicative of a loading situation with load factor of 2 (the full weight of the aircraft supported on a single wing structure).

This test has demonstrated that the wing spars can bear loading conditions with a load factor of 2. This load factor is more than the minimum load factor requirement of 1.15 inside the anticipated flight envelope. Hence, the wing design has been shown to be fit for purpose with a low risk of spar failure during the chosen flight envelope.

5.2 Wingbox Structural Testing

In ideal circumstances, extensive NDT (Non-Destructive Testing) would be carried out on the wing box structure, but with time constraints surrounding the build of the UAV, a decision was made by the team that the FEA analysis would have to be sufficient. This would be posted as high priority for further developments as the budget could allow for a second wing box to be printed for testing, with static loading tests being carried out on the forward, wing and tail spar. The validity of the FEA results have been proven in the wing structure testing, Section 5.1 and tail testing, Section 5.3 where the predicted deflections in physical testing have been achieved with no component failure.

5.3 Tail Structural Testing

To test if the tail section could withstand the stresses induced during flight, a physical tail test was conducted. The aim of the test was to evaluate the bending of the square cross section tail boom during a typical elevator deflection. A load of 7.84N has been calculated as outlined in document DES_FI_CALCS_001 and used to represent the force acting on the tail due to the elevator deflection. The test involves mimicking this force and qualitatively evaluating the deflection of the tail. The actual tail module was used for this test.

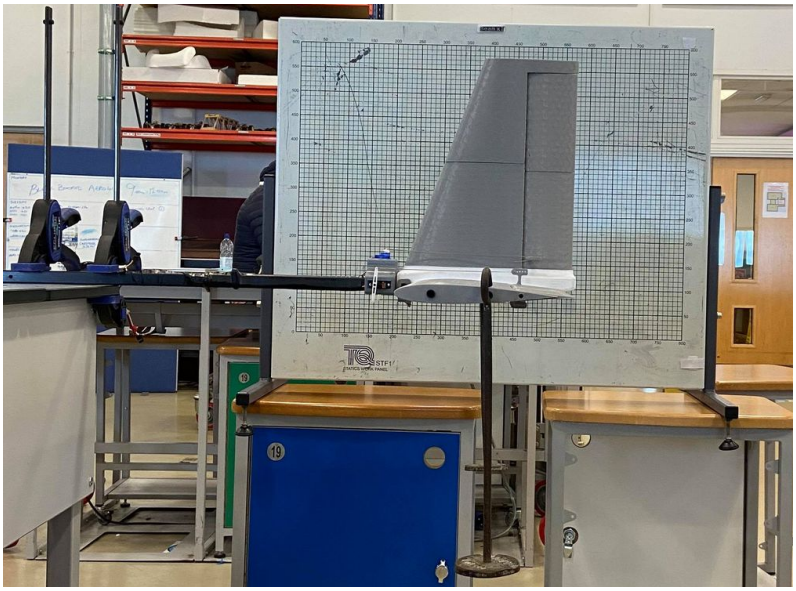

Figure 19 - Experimental set up and qualitive results of the physical tail testing

The following is the experimental set up and the method used to achieve the results shown in Figure 19:

- The actual tail module was clamped to the bench such that the clamped length of tail was the same length as that which is secured inside the wing box during a flight (140 mm) .
- Two 500 g masses were placed at each end of the horizontal tail, as close to the rear spar as possible (so the 3D printed tail structure was not damaged).
- These masses equate to a vertical force of 9.81 N acting vertically on the horizontal tail, representing a load factor of 1.25 (in relation to the predicted force).
- Figure 19 shows the resultant bending of the tail boom from this applied load.
-

Since the tail section did not catastrophically fail during this loading test it has been demonstrated that the tail boom can bear these loading conditions with a load factor of approximately 1.25. This load factor is greater than the minimum load factor requirement of 1.15 inside the anticipated flight envelope. Hence, the tail design has been shown to be fit for purpose with a low risk of failure during the chosen flight envelope. The anticipated flight envelope can be found in Appendix B.

5.4 Avionics Testing

5.4.1 Calibration

To be able to arm the UAV, the aircraft sensors, radio and flight modes have to be calibrated and/or defined.

5.4.1.1 Sensors

The compass is calibrated by following the onscreen instructions from the ground station. The graphical instructions request that the operator hold the Pixhawk 4 board in six orientations and rotates them counterclockwise. Figure 20 shows the six orientations, four of which have been calibrated (green border), one which has not been calibrated (red border) and one mid calibration (yellow border).

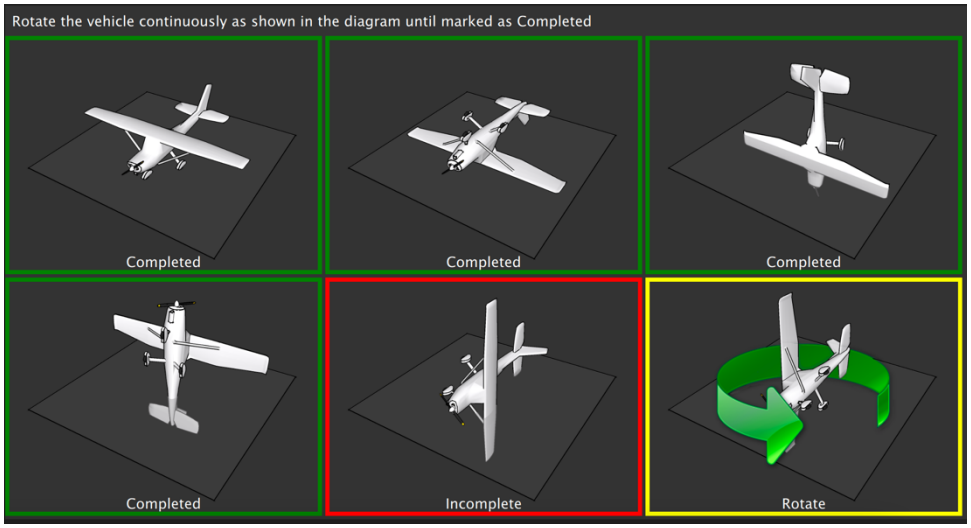

Figure 20 - Compass calibration screenshot from QGC

All other sensors are calibrated in a similar way to the compass outlined above with the exception of the airspeed sensor. The airspeed sensor is calibrated by following the onscreen instructions from QGC. It involves ensuring that the sensor is not measing any wind, and then blowing over the end of the pitot tube and ensuring a measurement of ≥50Pa is reached.

5.4.1.2 Radio

The radio is calibrated via graphical instructions from QGC. The user initiates the process through the computer and then completes a series of transmitter inputs in line with a picture on QGC. Once the radio is calibrated, the circle next to 'Radio' in the taskbar to the left of the screen will change from red text, to white. Figure 21 shows that the radio has been calibrated successfully.

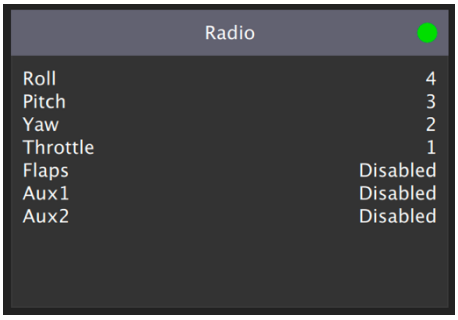

Figure 21 - Radio calibration complete

5.4.1.3 Flight Modes

The flight modes are defined by the user in accordance with document DES_TEST_BUILD_001. Figure 22 shows the standard configuration of the flight modes. Document AVI_TEST_FM_001 contains the test that ensures that all five flight modes can be selected via the transmitter. The results of this test were that the transmitter was capable of selecting all five flight modes.

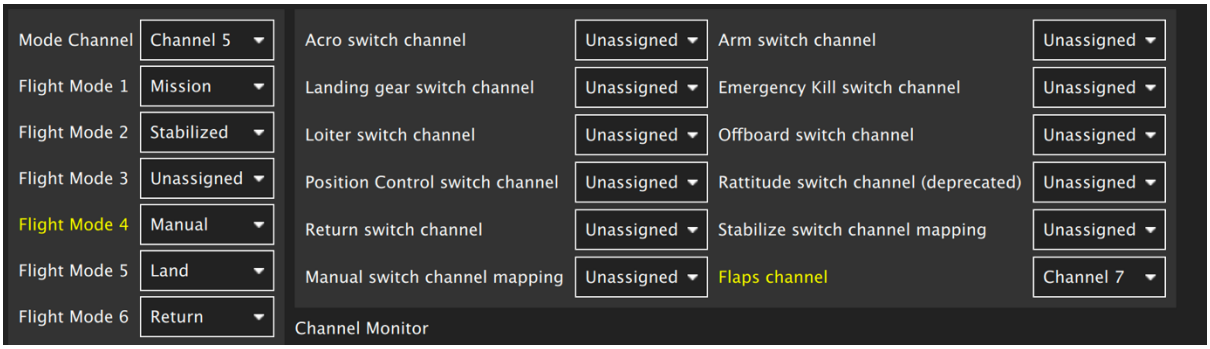

Figure 22 - Flight mode definitions

5.4.2 Avionics Actuation

To ensure that the inputs from the operator result in the expected physical outcomes/actuations on the UAV, a full avionics test must be completed prior to every flight. The full testing booklet can be seen in document AVI_TEST_AVI_001. This test ensures that all of the control surfaces (ailerons, flaperons, flaps, elevator and rudder) operate as expected and deflect in the desired direction. It also confirms that the gimbal and throttle operate as expected. This booklet was followed by a member of the team who had not been involved in the avionics and was able to confirm that all of the control surfaces operated as expected.

5.4.3 Circuit Testing

A multimeter was used to validate that there were no faults within the avionics circuitry. Continuity tests were performed on each of the individual wire sections to ensure that there were no shorts present within the circuit, and that no faults could be traced to faulty wiring. Checks were also made on each of the pins on the power distribution board – this ensured that both the correct voltages were being supplied to the ports, and that the various pins corresponded correctly (e.g. earth to earth). Furthermore, the voltage supplied by the batteries was also checked and verified after they had been fully charged.

5.4.4 GPS & Compass

To ensure that the UAV was able to connect to GPS and the compass was orientated correctly, the aircraft and the avionics components were taken outside into an open area. To confirm GPS connectivity, the ground station (QGroundControl) was connected, and it reported back that 5 satellites were connected. Figure 23a shows that the GPS had connected to 5 satellites, Figure 23b shows the compass orientated in direction one and Figure 23c shows the compass orientated 180° from direction one.

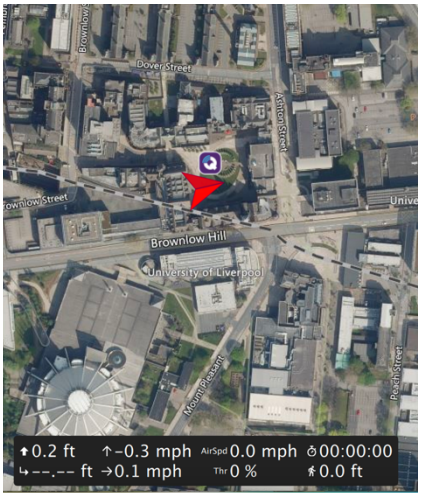

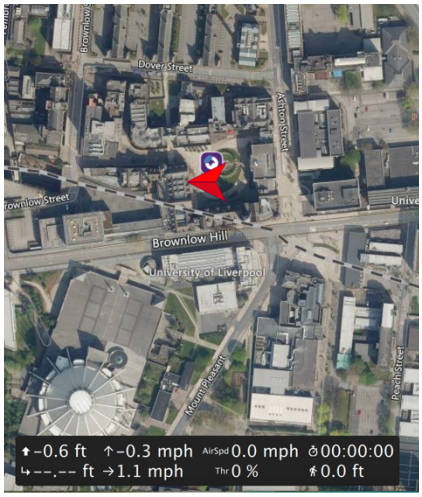

Figure 23 - 5 satellites connected (a - left), compass direction one (b - centre), compass direction two (c - right)

5.4.5 Control Surface Test Rig

Initially a control surface test rig was built by the team to identify any interfacing issues between the wing design and the avionic components. The initial test rig is shown in Figure 24a. This setup, although rudimentary, allowed the team to confirm that the electronic components and wing design could function as a successful subsystem. The team then produced a control surface with a full-scale chord length – Figure 24b – to scrutinise and develop a method of control horn and actuator arm size that would result in the desired deflection. This gave insight into issues relating to the orientation of the servo. Document AVI_TEST_CALCS_001 shows the complexities and precision required in constructing a control surface with the servo orientated as shown in Figure 25. For these reasons, a change control process, as shown in Figure 7, was undertaken.

Figure 24 - (a) First aileron test rig and (b) second aileron test rig

After this change, the team created a full-scale test rig to further develop the control surface subsystem. This rig is shown in Figure 25. The change resulted in a simpler system, where the servo deflection more directly mapped to the control surface deflection. More information can be found in document AVI_TEST_CALCS_001. The main outcome of this iteration was the decision to use two control horns instead of one; this helps to act as a failsafe for the system and ensures that the control surface has at least one actuator rod pulling in the desired direction. The rig also helped to establish that the optimum height for each control horn was 25mm.

The aileron test rig was tested in the wind tunnel to confirm that full control surface deflection was achievable up to and including VNE (20m/s) – this was verified. The fixing of the wing skin to the ribs was tested at the same time, and the structure remained in the same state as it was prior to the test. More information can be found in AVI_TEST_WIND_001.

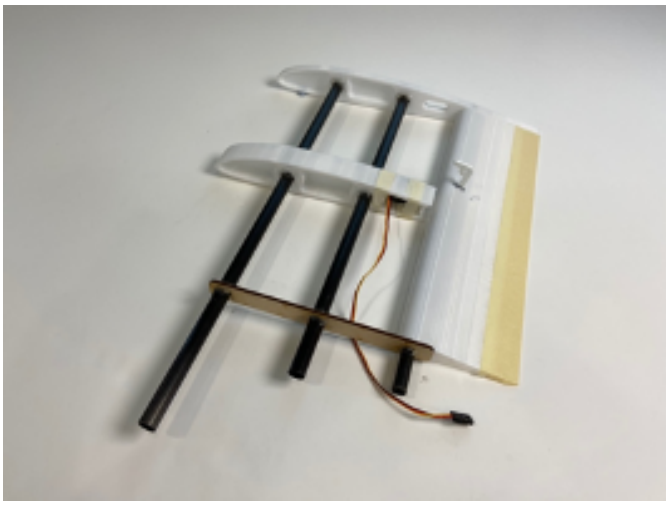

Figure 25 - Full scale aileron test rig with new servo orientation

From the previous iterations, it was deduced that the gluing method used to fix the control horn to the surface required excessive manual dexterity and could be designed more with DfM (Design for Manufacture) in mind. The team therefore decided that the control surface should be redesigned to directly incorporate the control horn, reducing the difficulty associated with assembly and improving the accuracy and consistency of the build. The final control surface design is shown in Figure 26.

Figure 26 - Final control surface design showing fully integrated control horn

5.4.6 Avionics Tray Sizing & Layout

An avionics tray (Figure 27a) was initially built by the team to be used in conjunction with the iron bird (images of the iron bird can be seen in document AVI_PL_AVI_001). This primitive tray allowed the team to design a layout of instruments and visualise the space available for placement. A secondary tray was then built, based on the CAD model design. This allowed the team to further refine the placement of the components and is shown in Figure 27b. A third iteration was then created (Figure 27c) in order to assess the mass of the tray and whether any mass reduction would be possible. It was deemed that the flat plate could be reduced in thickness to 1mm. The fixing method between the flat plate and support spars was also able to be changed to reduce mass.

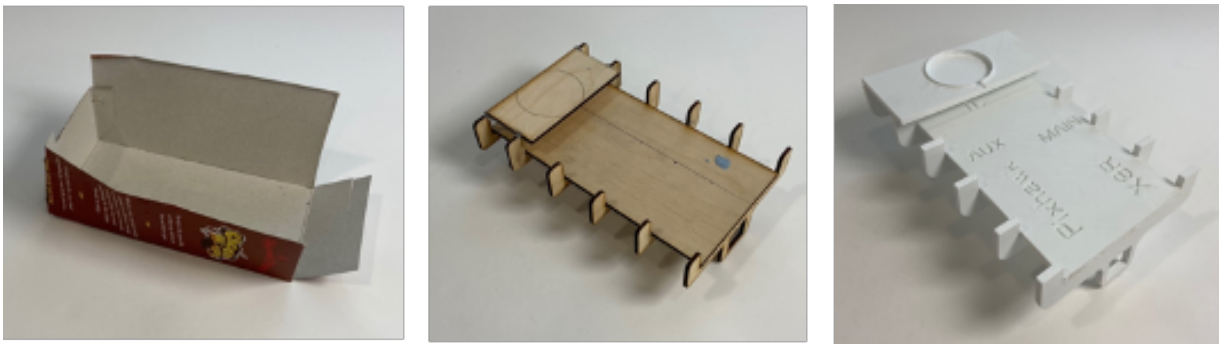

Figure 27 - Mk I (a - left), mk II (b - centre), mk III (c - right) avionics trays

5.5 Propulsion

Section 2.2.3 outlines the decisions made to determine which motor was to be chosen for the aircraft. The PO-3547-1190 with the accompanying APCE 11" x 5.5° propeller.

5.5.1 Motor Mount

The motor required a structurally optimised mount, this will transfer the thrust from the propeller through the central longitudinal beam running down the spine of the aircraft. The motor mount, as a CAD model, evolved throughout the whole manufacturing process. The addition of one centralised hole, added to the base plate, to accommodate the aft shaft on the motor, as well as the M3 holes, which were enlarged to account for the PLA shrinkage as it cools. The fundamental changes were how the part was printed. Initially the motor mount was PLA 3D printed at: a resolution of 0.2mm, 35% infill density, and a wall thickness of 2mm.

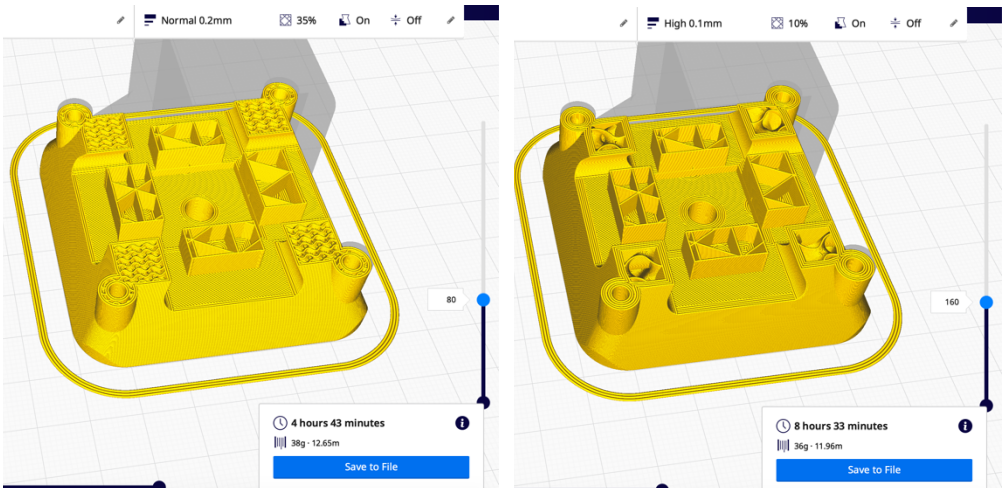

Figure 28 - Motor mount slicer comparison

The slicer software, Ultimaker CURA, was adjusted to print the component with a resolution of 0.1mm, 10% infill density, and a wall thickness of 4mm. A side-by-side slice comparison can be seen in Figure 28, where the quality of the print and density can be compared. The rapid prototyping of the motor subframe was apparent when a component failed due to miss assembly, it could be re-printed in under 9 hours. The final design was not only refined in print but was also modified to be pinned directly through the square carbon fibre structure using an M5 bolt and a nylon locking nut – as shown in Figure 29.

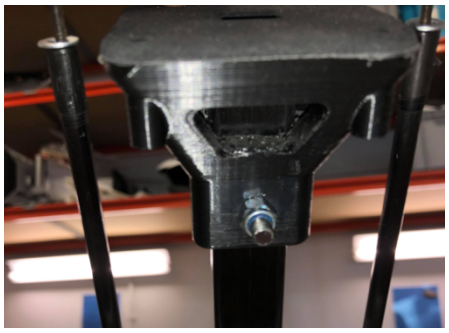

Figure 29 - Picture of motor mount with pin bolt connection

5.5.2 Additional Motor Support

The addition of the torsion plate, which is bolted to the motor subframe, allowed the team to secure the motor to a piece of metal. The 6mm thick Aluminium torsion plate was selected due to the high tensile strength per mass: 270-345 MPa (Alloy Sales, 2016), its high melt temperature: 570°C (Alloy Sales, 2016) and its corrosion resistant properties. Between the Aluminium torsion plate and the PLA motor subframe, and between the carbon fibre structure two pieces of neoprene have been sandwiched by the components to offer some passive vibration damping. The motor was spun, without the propeller, whilst bolted onto the airframe, where a qualitative 'feel test' was performed. The airframe was held by the main carbon structure to feel for any vibrations coming from the motor at full throttle. The airframe felt very little vibration in comparison to the test conducted previously without the neoprene layer for passive damping. The motor and propeller have both been professionally balanced by the manufacturer prior to shipping. On either side of the Aluminium torsion plate, carbon fibre rods from the wing box are rivlocked into tension from both sides of the motor itself, in order to give the system more rigidity.

5.5.3 Motor Tests

Drag was computed using the interpreted data from the wind tunnel test, as shown in the applicable document: SIM_TEST_WIND_001. To check the motor was suitable for this airframe, the drag value for an angle of attack of 15° (roughly 0.26 radians) was used. For the Clark-Y airfoil, which is the airfoil shape used in the airframe, stall and detached airflow can happen around 15° typically, therefore choosing 15° gives a minimum performance value. Using the drag formula, also found in SIM_TEST_WIND_001, the form drag plus the induced drag was computed at cruise velocity, assuming sea level density, is: 6.3 Newtons. As shown by the motor testing, the PO-3547-1190 motor and APCE 11" x 5.5° propeller produce up to 20.1N. This indicated that when flying at stall drag conditions, the motor has a factor of safety of 3.17, therefore is suitable for the mission.

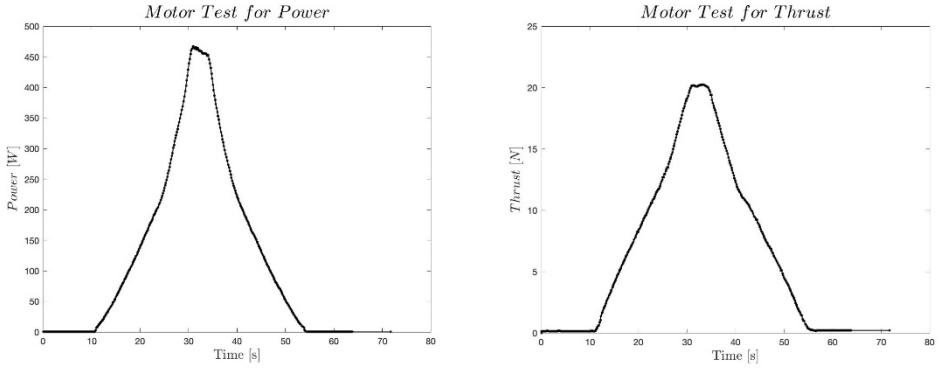

Figure 30 - Motor test results

5.6 Adhesive Testing

Three different types of adhesives were tested. There is a PLA to carbon fibre join required at every wing rib along both of the wings. These ribs are to support the wing skin and provide the airfoil shape to the wings. The control surface hinges rely on the structure of the ribs, as shown in Section 5.4.4, however the majority of the aerodynamic forces will act through the carbon fibre rods.

The three adhesives which were evaluated were: epoxy resin glue, polystyrene foam glue, and "Gorilla" Cyanoacrylate glue. All joins were tested by twisting the rod with a viced airfoil after the glue had hardened. The epoxy resin did very little towards fusing the two surfaces, polystyrene foam glue did bond, but the bond was brittle and could be broken easily. The superglue held the rod and wing rib connection successfully. The rod was twisted such that the rib was destroyed however the bonded surfaces remained fused to the rod as the rib broke around it.

The superglue was chosen to be used for these joins. The superglue also had the lowest mass by a considerable margin so the additional mass from the glue can be considered negligible compared to the wing structure. The Gorilla glue comes in 15g bottles, and the construction of the wings used approximately 1.75 bottles, which accounts to 26.3g of mass which is evenly distributed over the wings. The fully constructed wing was tested in a wind tunnel at 13 m/s in order to confirm the control surfaces were fully operational as part of the whole assembly. This test was carried out up to the 'V_{NE}' of 20 m/s in order to confirm that the glue is able to hold the wing surface on up to the maximum speed stipulated by the flight envelope (Appendix B). More information regarding the wind tunnel can be seen in document AVI_TEST_WIND_001.

5.7 Wind Tunnel Testing

The plots in Figure 31 were generated in the Wind Tunnel using a 10% scale model (Figure 31), for the purpose of comparison to analytical results. This complimented the Simulink model. They demonstrate a lack of expected stall behaviour, hence only the linear region can be relied upon. Using equation 1, the C_D vs α plot was obtained. The methodologies behind this process can be found in SIM_TEST_WIND_001.

$$C_D = C_{D_0} + kC_L^2 \qquad 1$$

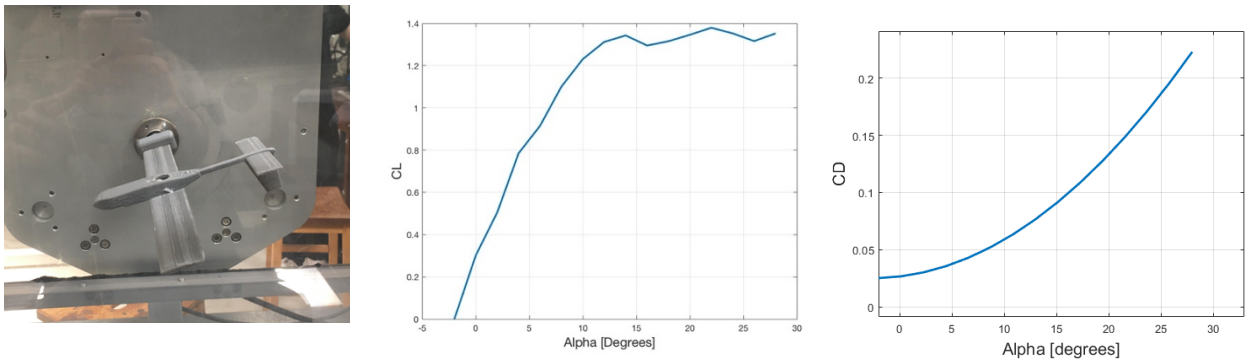

Figure 31 – 10% scale model in wind tunnel (left), wind tunnel testing results (CL – centre), (CD – right)

5.8 Payload Testing

5.8.1 Gimbal Testing

The primary objectives of the gimbal test were to ascertain: the maximum deflection angle; the time it took for the gimbal to rotate between maximum deflection in either direction; and to test the servo torque capability. The mission requires 46° of gimbal rotation in each direction from the vertical position. It took 0.7 seconds to rotate from maximum left to maximum right position – this ensures the camera is capable of capturing images perpendicular to the cliff. As the aircraft will be primarily conducting rate 1 turns during the survey, the time period required for full gimbal deflection is sufficient. Further details of the test are illustrated in supporting document PAY_GIMBAL_TEST_001. Figure 32 shows the gimbal deflecting 46° in either direction whilst the camera is in-situ.

Figure 32 - Pictures of gimbal at maximum deflection during timing test

5.8.2 Camera Testing

Camera testing was completed to create a GSD comparison at increasing distances from a calibration board, and to create a set of recommended settings for the customer. The test involved taking pictures of the calibration board over 60m in 5m intervals. At 60m (the largest perpendicular distance that the aircraft would be from the cliff face) the GSD was theoretically calculated to be 0.5126cm/px, however during testing, a GSD of 0.5208cm/px was achieved. This was within the customer requirement of 0.82cm/px. The tests concluded that the highest quality images for daytime flight were:

- ISO set to 100.
- Exposure between 1/80 and 1/2500 depending on daytime brightness.
- An aperture between f/1.8 and f/9.

Full details of the camera test can be seen in supporting document PAY_CAMERA_TEST_001, whereas camera settings research and testing can be seen in supporting documents PAY_CAMERA_TEST_002 and PAY_CAMERA_TEST_003. Images of the calibration board taken at 5m and 60m can be seen in Figure 33.

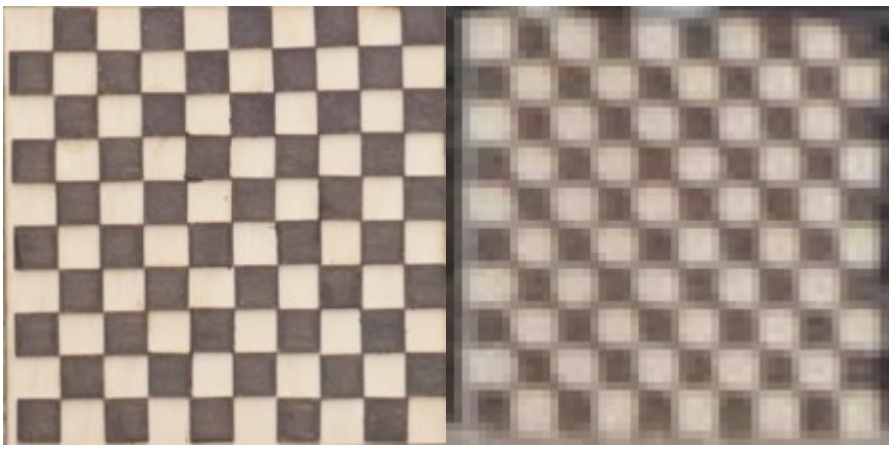

Figure 33 - Testing images calibration board at 5 meters (left) and 60 meters (right)

5.9 Packaging Tests

To allow the aircraft to be transported safely and securely, packaging boxes have been handmade using recycled cardboard. This is an eco-friendly, sustainable solution and allows the team to utilise spare budget resources elsewhere. There are three boxes in total, each uniquely built to fit the main components of the aircraft: the main wings, the wingbox and the tail section – the boxes are shown in Figure 34a below. Each box was spray painted black and labelled accordingly. Custom foam inserts (Figure 34b) were created in order to house the components safely inside the boxes, and Velcro straps were added. The team acknowledged the large size of the boxes, and subsequently liaised with the customer on suitable methods of transportation; through this, it was determined that the customer would be using a van to access the test site, and thus the boxes would not present any challenges in this regard. If a van is not readily available for future transport of the aircraft, the team has verified that the boxes will fit inside a regular sized car, assuming there are no other passengers present.

Figure 34 - (a) Bespoke packaging solution boxes and (b) foam inserts for the main wing box

In order to test the suitability and effectiveness of the boxes, tests were performed in line with British Standard EN 15552:2008. This document details specified testing schedules that help determine whether packaging meets international standards – it can be found in PKG_TEST_RISK_001. A sample of the tests listed in this document were carried out by the team, with each test being performed on all three boxes individually, with the relevant components secured inside.

Stacking tests were performed using a dead load in order to investigate the effects of compression stresses applied to the boxes. Results found no permanent deformation to the boxes, and no damage to the components within. Similarly, the boxes were stacked on top of each other to mimic a possible real-life transportation setup – again, no deformation or damage to the boxes or components was observed, validating the structural integrity of the packaging build. Vibration tests were performed using random vibrations (EN ISO 13355) to best reproduce the vibration stresses experienced during transportation. Slight movement of the parts was noticed during this test, thus remedial actions were taken to improve the security of the parts within the box; the foam inserts were glued to the boxes (where possible) to prevent further movement, and the shapes of the foam parts were refined and re-cut so that the components would fit more tightly and accurately within. Furthermore, vertical and rotational drop tests were carried out to investigate the effect of impact hazards. This entailed dropping the boxes from a height of 2ft, both vertically and with some rotational force. After multiple iterations of the test, it was verified again that no damage occurred to the boxes or components, thus concluding that the boxes could withstand potential impact loading during transportation and handling.

6 Flight Test Plan

To ensure the aircraft is capable of completing the mission successfully, a series of flight tests will be completed. Initially a static systems test will be conducted to check all of the subsystems are operating as expected by the team. This was conducted in line with document AVI_TEST_AVI_001.

Once the systems test has been successfully completed and the team has confirmed the UAV operates as specified in the pre-flight checks, a series of test flights will be conducted. The test flight will operate in accordance with the CAP 393 Air Navigation Order and must adhere to Articles 94 and 95 as flying outside such legislation would require permission of the CAA. The (UAS operator qualified) drone pilot will operate the drone in a pre-planned mission at the Wyncote Sports Field. The flight paths have been designed to not infringe on the legal 50m distance required between any nearby people, vessel, vehicle or structure not under the control of the operator. This flight plan includes a geofenced perimeter which will automatically return the UAV to the rally point if it goes beyond the specified boundary.

The flight test will consist of two rejected take offs followed by a manual take-off and landing with an autonomous flight circuit. The only subsystem which will not be tested during the first flight test is the camera trigger. This is due to the fact that a dummy camera will be employed on this flight test to mitigate any risk of camera damage on the first flight. A final test flight will be performed where the platform will test its ability to survey a specified area, the images gathered will then be analysed to ensure they satisfy the customer requirement for images of sufficient resolution (OCDR1). A flight test specific risk register can be found in document MNGT_FI_RISK_002 and must be reviewed before carrying out the test procedures.

6.1 Static Systems Test

The static systems test has been completed by the team to confirm the UAV operates as expected and should be completed after every assembly. This test confirms that:

1. The UAV can be constructed via the use of the instructions, in document DES_TEST_BUILD_001.
2. The ailerons deflected a maximum of 30° in both directions.
3. The ailerons act as equal and opposite and deflect in the desired direction.
4. Both the flaps and flaperons deploy equally on both wings.
5. The rudder deflects a maximum of 30° in both directions.
6. The elevator deflects a maximum of 30° in both directions.
7. All of the switches allocated on the transmitter result in the desired effect on the aircraft.
8. The gimbal deflected a maximum of 46° in both directions.
9. The camera can be triggered remotely and can take photographs on demand.

Each of these were tested individually and the team were able to confirm that all of these subtests were passed. Documents AVI_TEST_AVI_001 and DES_TEST_BUILD_001 outline the processes taken to confirm each of these capabilities.

6.2 Flight Test

6.2.1 Rejected Take-off Tests

Prior to the flight tests there will be a low and high speed rejected take off run performed. This will consist of testing the UAV and its landing gear on the runway that will be used for the flight. This will allow the pilot and team to observe any uneven terrain and familiarize themselves with the controls before the flight tests.

1. Clear runway of any debris and ensure the flight zone is clear of pedestrians.
2. Manually align the UAV with the centre of the runway.
3. Ensure flaps are in the up position.
4. Increase throttle position until it reaches a speed of 5m/s.
5. Decrease throttle to idle.
6. Inspect the aircraft for any damage.
7. Repeat test at 10m/s.

6.2.2 Flight Test 1

Subject to the success of the rejected take off, two flight tests have been planned by the team to ensure that the UAV is capable of carrying out the final mission. The first flight test will consist of a manual take-off and landing with an autonomous flight circuit at Wyncote Sports Fields. The flight test has been planned in QGroundControl and is shown in Figure 35. It will consist of a 26 second flight with a take-off, climbing to an altitude of 15m and landing with a glide slope of 7.1°.

1. Clear runway of any debris and ensure the flight zone is clear of pedestrians.
2. Manually position platform is parallel and on the runway (Waypoint L).
3. Upload the QGroundControl flight plan file.
4. Ensure flaps are in the down position.
5. Increase throttle position until it reaches a speed of 12m/s.
6. Allow the aircraft to reach 15m altitude (Waypoint 2).
7. Switch Taranis to Autonomous flight mode.

8. Switch to Manual flight mode as UAV approaches for landing (Waypoint 8).

Figure 35 - Take-off and landing (flight test plan 1)

To mitigate against any risk of expensive payload damage, a dummy camera will be used as a placeholder for the Sony A5000. The dummy camera is a 3D printed model of the exact camera, hollowed out with weights inside to replicate the camera used in the customer mission. An image of the dummy camera is shown in Figure 36.

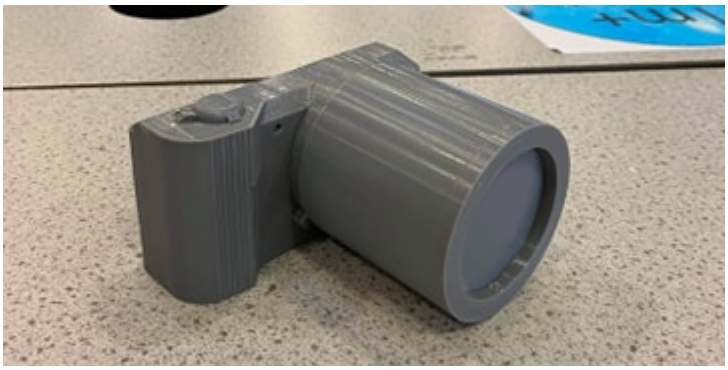

Figure 36 - 3D printed dummy camera

6.2.3 Flight Test 2

Subject to the success of the first flight test a second will then be conducted with the camera installed. This will be an extended flight test consisting of take-off, climb to 30m altitude, survey the specified area shown in QGroundControl and the landing. For this a camera resolution testing board will be placed in the survey area to determine if the camera is capable of capturing the images of sufficient resolution.

Figure 37 - Take off, survey and landing (flight test plan 2)

1. Clear runway of any debris and ensure the flight zone is clear of pedestrians.
2. Manually position platform is parallel and on the runway (Waypoint L).
3. Upload the QGroundControl flight plan file.
4. Ensure flaps are in the down position.
5. Increase throttle position until it reaches a speed of 12m/s.
6. Allow the aircraft to reach 15m altitude (Waypoint 2).
7. Switch Taranis to Autonomous flight mode.
8. Enable camera survey mode on QGrouncontrol.
9. Switch to Manual flight mode as UAV approaches for landing (Waypoint 8).

The flight test risk register (MNGT_FI_RISK_002) should be reviewed before undertaking the flight tests to inform the pilot of the risks which have been identified by the group, the top three risks are shown in Figure 38.

AERO420 Group Design
Flight test Risk Register

UID	Originator	Probability	Severity	Risk	Description	Mitigation	Contingency
N/A	-	1	1	1	Highly unlikely, Negligible impact	Factors put in place to reduce the likelihood of the risk occuring	Factors put in place as a 'workaround' if risk were to occur
N/A	-	2	2	4	Unlikely, Minor impact		
N/A	-	3	3	9	Moderate likelihood, Moderate impact		
N/A	-	4	4	16	Likely, Significant impact		
N/A	-	5	5	25	Highly likely, High impact		
3	Oliver	1	5	5	UAV colision with person or property	Ensure flight zone is clear of pedestrians and all participants are aware of the UAVs position. Put in place Geofencing and return to home feature	Insure the UAV against damages
2	Oliver	3	3	9	Loss of control of the UAV	Carry out the familiarisation tests before the flight. Read the pilot notes before flying the UAV and operate within the stated limits	Ensure Qgrouncontrol flight stability is enabled
1	Oliver	3	4	12	Crash during landing or take off	Carry out flight test in optimal weather conditions. Carry out preliminary static tests and aborted take-offs. Ensure pilot has undergone training and has sufficient experience. Clear the runway of debris	Design flight plan with large open spaces at both the take off and landing waypoints

Figure 38 - Flight test risk register top three risks identified

6.2.4 Flight Test 3

The team is currently pursuing permission from the RAF to use the RAF Woodvale private airport to carry out further flight tests. While the aforementioned flight tests operate within the CAA legislation, the risks shown in document MNGT_FI_RISK_002 for the proposed location at Wyncote are far greater than the risks associated with equivalent flight tests at RAF Woodvale. This would also allow for a more thorough testing of the UAVs capabilities.

In conclusion the team have decided that the preferred test location is RAF Woodvale. This is due to there being more space available to operate in and the facilities are purpose built for conducting flight tests.

7 Risk & Mitigation

7.1 Risk Register

Throughout the project, a live risk register has been hosted on the team's cloud storage system. This has allowed all members of the team to view and contribute any risks identified throughout the duration of the project.

Allowing the whole team to access and append risks has ensured the breadth of perspective required of a successful risk survey. As each team has had specialised objectives, they have been able to easily identify, record and notify other team members of these risks. The risk register document can be found within document MNGT_FI_RISK_001.

The risks were initially identified and assigned a Unique Identification Number (UID). They were then scored out of 5 in terms of their likelihood (chance of occurrence) and severity (how severe is it if the risk occurs). These two scores were then multiplied together giving an overall risk score. This number was then used to score all of the risks and assign them to groups based on priority. Both a mitigation and contingency plan were put in place for all of the risks and the originator was responsible along with the principal engineer for ensuring either/both were carried out at the relevant time.

Shown in Figure 39 are the top three scoring risks which posed a threat to the success of the project.

One risk materialised into a threat throughout the duration of the project, this was risk 7. Due to this risk occurring, the contingency plan was activated, and the group were able to resolve the issue and continue on the projected path to completion.

UID	Originator	Probability	Severity	Risk	Description	Mitigation	Contingency
N/A	-	1	1	1	Highly unlikely, Negligible impact	Factors put in place to reduce the likelihood of the risk occuring	Factors put in place as a 'workaround' if risk were to occur
N/A	-	2	2	4	Unlikely, Minor impact		
N/A	-	3	3	9	Moderate likelihood, Moderate impact		
N/A	-	4	4	16	Likely, Significant impact		
N/A	-	5	5	25	Highly likely, High impact		
1a	George	3	5	15	Covid 19- closure of labs	N/A	Increase simulation aspect of the project
6a	Amanda	3	4	12	CAA approval declination	Seek guidance from module teaching staff and ensure that paperwork is completed and submitted early on in the project life cycle to alow for any changes to be made to the design	Enable UAV to be controlled by both user input and autonomous flight computers
7	George	3	4	12	Software issues as all software being used is open source	Ensure all software is up to date	Allocate an individual/team to resolve the issue, either by finding alternative software, contacting the software developers or seeking guidance from teaching staff

Figure 39 - Top three ranking risks posing threat to the success of the project

7.2 Checklists

As customer acceptance is the final goal of the project, a comprehensive checklist system has been developed by the team to ensure that the customer is able to operate the UAV both safely and effectively. The checklists have been cross referenced with published materials to ensure consistency in all key areas. Figure 40 highlights some of the contents within the checklist. The entire document for the UAV can be seen in document DES_PL_ALL_003.

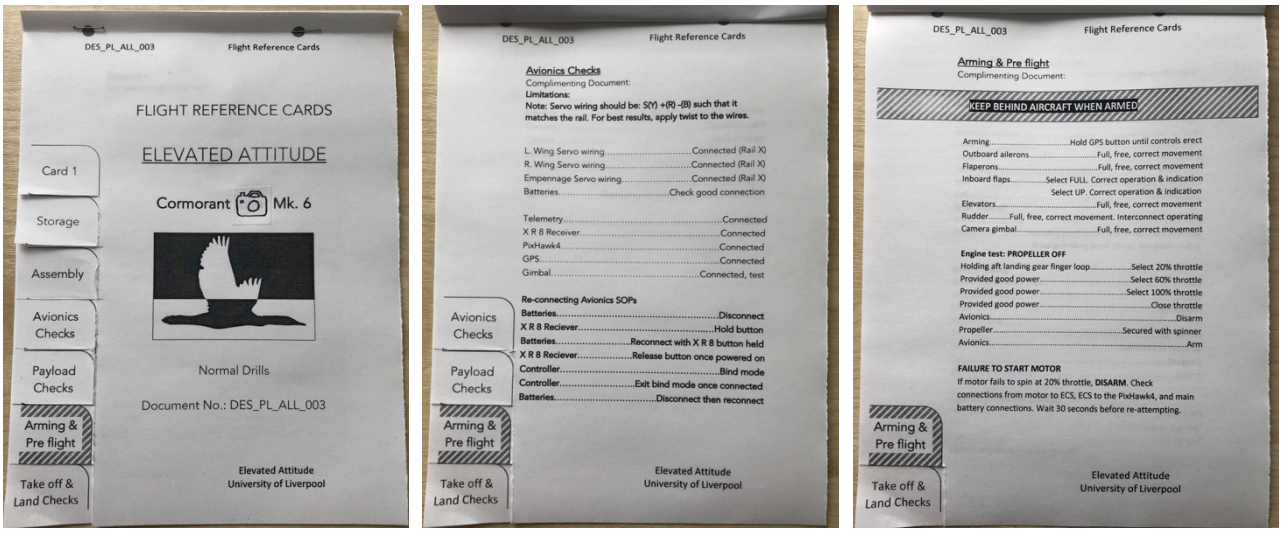

Figure 40 - Flight checklists for UAV

As shown in Figure 40 the checklist covers a broad range of aspects including unpacking the modules, combining them correctly to build the UAV, operation, emergency procedures, deconstruction and repacking. This manual ensures that the customer has in depth documentation to refer to during the use of the UAV, allowing them to use the UAV safely and effectively.

An illustrated step by step will also be provided in conjunction with the written checklist. This will mainly focus on the building and deconstruction aspects of the UAV modules. Having an illustrated

instruction manual will aid in the safe building of the UAV, it also eliminates any language barriers during the build which lends itself to the reusability aspect of the surveying platform.

A colour coding system has been used to allow ease of connection of the components and reduce any error associated. With this said, if the customer was to crosswire the control surfaces, the pre-flight checks would mitigate this and ensure the aircraft is set up correctly and calibrated prior to flight.

8 Budget

The budgets for the avionics, payload and airframe are shown in Tables 5, 6 and 7 respectively. This totals to £638.03 leaving a remaining balance of £361.97 of the £1000 budget.

Spending of the surplus could be used to:

- Destructive wingbox testing.
- Additional spare components.
- Higher quality camera.
- Longer range avionics.
- Purchase freeware equivalents.
- Higher quality packaging solution.
- Destructive carbon rod testing.
- The hire of a vehicle for easier transport on the day of the survey.

Table 5 - Avionics Budget

Avionics	Quantity	Cost	University?	Actual Cost
Pixhawk 4	1	£179.95	✓	£0
Servo	8	£78.67	-	£78.67
Motor	1	£35.99	-	£35.99
Prop	1	£4.30	-	£4.30
Telemetry set	1	£39.95	✓	£0
Patch antenna	1	£4.99	-	£4.99
GPS module	1	£37.27	✓	£0
Battery	2	£134.98	✓ x1	£67.49
ESC	1	£17.99	✓	£0
Pitot tube	1	£31.50	✓	£0
Total		**£565.59**		**£191.44**

Table 6 - Payload budget

Payload	Quantity	Cost	University?	Actual Cost
Camera	1	£449	✓	£0
Lens	1	£159	-	£159
Servo	1	£20.99	✓	£0
Memory card	1	£18.99	✓	£0
Adapter cable	1	£43.53	✓	£0
Total		**£691.51**		**£159.00**

Table 7 - Airframe budget

Airframe				
Longitudinal Spars	2	£51.60	-	£51.60
Lateral Spars	4	£67	-	£67
Wingbox Print	1	£60	-	£60
Various Fixing Methods	12	£25	-	£25
PLA/PLA+	2kg	£44	-	£44
Landing Gear	1	£39.99	-	£39.99
Total		**£287.59**		**£287.59**

Bibliography

Alloy Sales, 2016. *6mm Aluminium Plate.* [Online]
Available at: https://www.alloysales.co.uk/3000-mm-x-1500-mm-x-6-mm-5083-aluminium-plate
[Accessed May 2021].
Easy Composites, 2021. *12mm pultruded carbon fibre tubing.* [Online]
Available at: https://www.easycomposites.co.uk/12mm-pultruded-carbon-fibre-tube
[Accessed May 2021].

Available at: https://www.scielo.br/scielo.php?script=sci_arttext&pid=S2175-91462019000100323
[Accessed 03 2020].
Delev, I., 2015. Advantages and Disadvantages of Using Open Source Software. [Online]
Available at: https://www.webhostface.com/blog/advantages-and-disadvantages-of-open-source-software/
[Accessed 5th March 2020].
Green, J., 2020. Counting Cormorants, s.l.: s.n.
I.Buchmann, 2021. Advantages and disadvantages of different types of batteries. [Online]
Available at: https://batteryuniversity.com/learn/archive/whats_the_best_battery
[Accessed March 2021].
Ioannou, S. et al., 2016. Runtime, capacity and discharge current relationships for lead acid and lithium batteries. Athens, Institute of Electrical and Electronics Engineers Inc.
Sadraey, M. H., 2013. Aircraft Design: A Systems Engineering Approach. 3 ed. New Hampshire: John Wiley & Sons.
SKYbrary, 2017. Flaperons. [Online]
Available at: https://www.skybrary.aero/index.php/Flaperons
[Accessed 7th March 2021].

9 Appendix

A – Simulink model

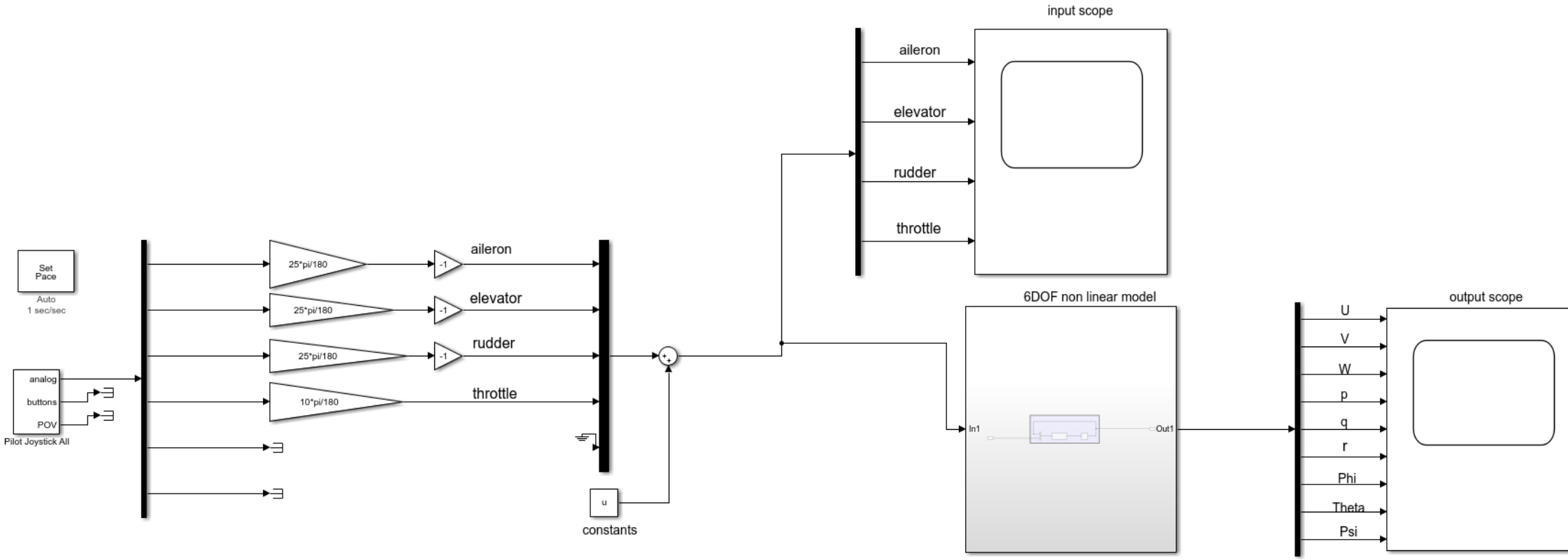

B – Flight Envelope